Journal of Catalysis 285 (2012) 223–234

Contents lists available at SciVerse ScienceDirect

Journal of Catalysis

journal homepage: www.elsevier.com/locate/jcat

TiO_2 photocatalyst for degradation of organic compounds in water and air supported on highly hydrophobic FAU zeolite: Structural, sorptive, and photocatalytic studies

Yasutaka Kuwahara [a], Junya Aoyama [a], Keisuke Miyakubo [b], Taro Eguchi [b], Takashi Kamegawa [a], Kohsuke Mori [a], Hiromi Yamashita [a,*]

[a] Division of Materials and Manufacturing Science, Graduate School of Engineering, Osaka University, 2-1 Yamadaoka, Suita, Osaka 565-0871, Japan
[b] The Museum of Osaka University and Department of Chemistry, Graduate School of Science, Osaka University, 1-16 Machikaneyama, Toyonaka, Osaka 560-0043, Japan

ARTICLE INFO

Article history:
Received 1 June 2011
Revised 23 September 2011
Accepted 24 September 2011
Available online 5 November 2011

Keywords:
TiO_2
Photocatalyst
Faujasite zeolite
Hydrophobicity/organophilicity
Dealumination

ABSTRACT

Preparation of highly hydrophobic FAU zeolite has been achieved by a two-step preparation method that comprises predealumination treatment using concentrated mineral acids and subsequent calcination treatment. The hydrophilic/hydrophobic character of the zeolites was estimated by detailed adsorption measurements using water and toluene molecules as adsorbates, which showed the strict hydrophobic nature of the prepared FAU zeolites. By means of TG, FT-IR, and ^{29}Si MAS NMR analyses, it was concluded that the enhancement in hydrophobicity originates from the healing of silanol defect sites and the formation of a refined silica surface with fewer adsorption sites. Thus-prepared FAU zeolite, with high crystallinity, structural and thermal stability, and hydrophobicity, significantly improved the photocatalytic degradation rates of 2-propanol in water and acetaldehyde in air on TiO_2 when it was used as a catalyst support. A distinct correlation was found between the hydrophobicity of zeolites and photocatalytic activity of the supported TiO_2.

1. Introduction

TiO_2 is currently considered the most promising catalyst for the photocatalytic degradation of organic compounds owing to its suitable band gap energy for redox reactions, mechanical and chemical stability, environmental friendliness, low cost, and convenience of preparation [1–4]. Given the current concern with environmental issues, it is anticipated that applications for TiO_2 will be growing at increasing speed, and in particular, urgent improvement of the TiO_2 photocatalytic degradation is potentially needed for large-scale industrial treatment processes such as waste water treatment and de-NO_x. However, there remain further technological problems, which may include easy separation of the catalyst and improvement of adsorption properties for organic molecules at low concentrations in the media.

Combining adsorbents (e.g., zeolites and mesoporous silicas) and TiO_2 photocatalysts makes it possible to create advanced photocatalytic systems with improved adsorption and condensation properties—for example, abatement of air and water pollution using solar light, as well as photooxygenation of hydrocarbons, de-NO_x processes, and other photochemical processes of concern in environmental sciences [5–9]. Our previous studies, which dealt with the photocatalytic degradation of organic molecules diluted in air and water, have systematically revealed that the photocatalytic activity of TiO_2 strongly depends on the hydrophobic character of the adsorbents in this type of hybrid photocatalytic system [10,11].

The hydrophobic/organophilic character of high-silica zeolites has been long recognized [12,13]. Owing to their excellent chemical, thermal, and hydrothermal stability, as well as their sieving properties, hydrophobic zeolites have found numerous applications in adsorption, separation, and purification processes in aqueous media [14], where their excellent affinity for hydrocarbons facilitates the mass transfer of organic substrates, inhibiting the adsorption of water molecules. The degree of hydrophobicity of zeolites is directly dependent on their Al content, i.e., the SiO_2/Al_2O_3 ratio of the zeolite framework, and on the related adsorption sites, such as Brønsted and Lewis acid sites as well as exchangeable cation sites. Silanol groups in the zeolite framework created by specific treatments and on the surface of mesoporous silicas have also been considered to work as weak adsorption sites for water molecules through hydrogen bonding [15,16]. It is thus of great importance to reduce such defect sites for preparing hydrophobic silicate adsorbents.

For example, the aluminum content of zeolites can be adjusted to some extent during the hydrothermal synthesis; however, among the numerous kinds of zeolites, the number of zeolite structures that can be readily synthesized as pure-silica or high-silica

* Corresponding author.
E-mail address: yamashita@mat.eng.osaka-u.ac.jp (H. Yamashita).

0021-9517/$ - see front matter © 2011 Elsevier Inc. All rights reserved.
doi:10.1016/j.jcat.2011.09.031

forms has been limited (e.g., ZSM-5 and ZSM-11), and most high-silica zeolites require the use of an organic structure-directing agent (SDA) in their synthesis. From an economic standpoint, this organic SDA is often the most expensive component in the synthesis, which limits the number of hydrophobic zeolites that are available commercially. The majority of commercially available zeolites at present are the ones that can be synthesized in the absence of SDA, such as LTA, FAU, and MOR zeolites, and hydrophobic zeolites are generally prepared by postsynthetic dealumination procedures. Dealumination can be accomplished by steaming treatments [17–19], acid leaching [20–22], and chemical treatments with chelating agents (EDTA, etc.) [23,24], silicon tetrachloride ($SiCl_4$) [25], and silicon hexafluoride [26]. Upon dealumination, the treatment conditions must be systematically adjusted for the composition, structure, and texture of the parent material in order to preserve the integrity of the crystallinity. Most of the industrial interest in dealumination of zeolite has been focused on its improved acidity [27], however, and little attention has been paid to the effect on hydrophobicity. To date, only a few papers have been devoted to the pursuit of the hydrophobicity of zeolites, e.g., BEA [28] and MOR [29].

We report here on an easy method for preparing extremely hydrophobic FAU zeolite. FAU zeolite (referred to as X- or Y-zeolite according to the SiO_2/Al_2O_3 ratio) possesses three-dimensionally connected microchannels consisting of supercages with diameter of ~1.30 nm and bridging tunnels with a widest diameter of ~0.74 nm, and the high sorption capacity and excellent mass transfer properties thus created allow multiple applications in industry as adsorbent, catalyst support, and solid acid catalyst [27,30]. Unfortunately, high-silica FAU zeolite cannot be directly synthesized due to the synthetic limitations of the Si/Al ratio (its naturally occurring Si/Al ratio is between 1.0 and 3.0). Therefore, it has been necessary to carry out repeated postsynthetic dealumination treatments in order to obtain highly siliceous FAU zeolite [31,32]. However, in the mass production of hydrophobic zeolite, chemical treatments using organosilanes or chelating agents that lead to waste streams should be avoided, from an environmental point of view. Our efforts systematically revealed that the hydrophobicity of FAU zeolites can be drastically improved via a two-step method, which consists of treatment of the as-synthesized zeolite precursor with a concentrated mineral acid solution and subsequent calcination at high temperature (T = ca. 1000 °C). The effect of treatment conditions (acid concentration, kinds of acids, temperature, and zeolite topologies) on dealumination kinetics was investigated by chemical, structural, and sorptive analyses associated with the surface environment of the zeolite, which was analyzed by TG, FT-IR, and ^{29}Si MAS NMR measurements.

Furthermore, making the best use of the hydrophobic/organophilic nature of the FAU zeolite thus obtained, it was utilized as a support material for TiO_2 photocatalysts, with the objective of fabricating efficient photocatalytic degradation systems for organic compounds diluted in water and air. The photocatalytic activity of the prepared samples was examined using photocatalytic degradation of 2-propanol in water and acetaldehyde in air under UV light irradiation as model reactions. Specific attention is paid to the correlation between the photocatalytic activities and the hydrophobicity of the zeolites, which is closely related to the adsorption kinetics of the adsorbates and the surface environment created during the acid and thermal treatments.

2. Experimental

2.1. Materials

Na-type FAU zeolites with SiO_2/Al_2O_3 = 5 (denoted as NaY(5)) and proton-type FAU zeolites with SiO_2/Al_2O_3 = 6.0, 13, 36, 54, 92, and 810 (denoted as HY(x); x is the SiO_2/Al_2O_3 ratio) were kindly donated by Union Showa K. K. HY(5.8) zeolite was prepared from NaY(5) by a standard ion-exchange procedure using aqueous ammonium nitrate solutions, followed by a repeated standard steaming process at 400 °C under 100% water vapor flow. Other types of zeolites such as MOR(15), ZSM-5(38), and Beta(20) were donated by Tosoh Co. Ltd. All zeolite materials were used as received without further washing or calcination. The TiO_2 powders, P-25 (consisting of 80% anatase and 20% rutile phases) and ST-01 (anatase 100%), were purchased from Ishihara Ind., Ltd. Ammonium titanyl oxalate ($(NH_4)_2[TiO(C_2O_4)_2]\cdot 2H_2O$; purity >98%), a titanium source for TiO_2, was purchased from Wako Pure Chemical Ind., Ltd. Acids, solvents, and all commercially available organic compounds for catalytic reactions were purified using standard procedures.

2.2. Preparation of hydrophobic zeolites

Acid leaching treatment was carried out by immersing zeolites in an aqueous mineral acid solution under reflux conditions. Typically, 3.0 g of HY(5.8) zeolite was suspended in 90 mL of aqueous nitric acid solution and was refluxed for 12 h with stirring. To provide a comparison, the nitric acid concentration was varied from 0.1 to 4.0 N, and the same procedure was conducted using 2.0 N aqueous solutions of hydrochloric acid, sulfuric acid, phosphoric acid, and acetic acid. After 12 h of reflux, the zeolite was recovered by filtration, washed several times with deionized water until complete elimination of the acid was achieved, and then dried at 110 °C overnight. Then, the resulting materials were calcined for 6 h in air at 400–1000 °C. Thus, obtained samples were denoted as deAl_T-Y, where T is the calcination temperature (°C).

2.3. Preparation of TiO_2/zeolite photocatalyst

The zeolite-supported TiO_2 photocatalysts were prepared by a standard impregnation method. To exclude the effect of thermal pretreatment on the hydrophobicity of zeolites, all zeolite samples were calcined at 1000 °C for 6 h at a heating rate of 1.5 °C/min in air before TiO_2 loading. Typically, 1.0 g of proton-type zeolite was suspended in 60 mL of aqueous ammonium titanyl oxalate solution (2.3×10^{-2} M) and was stirred at room temperature for 6 h, followed by evaporation of water under vacuum and calcination at 600 °C for 6 h with a heating rate of 1.5 °C/min in air. The TiO_2 content was fixed to be 10 wt.% according to our previous studies [10,11].

2.4. Characterization

Powder X-ray diffraction (XRD) patterns were recorded using a Rigaku Ultima IV diffractometer with Cu Kα radiation (λ = 1.54056 Å). Relative crystallinities of zeolites were determined by comparing the sums of the intensities of diffraction peaks in XRD patterns, assuming that of the starting zeolite material to be 100%. The global and framework Si/Al ratios were determined by inductively coupled plasma (ICP) measurement and by ^{29}Si MAS NMR, respectively. Nitrogen adsorption and desorption isotherms were measured at −196 °C using a BELSORP-max system (BEL Japan, Inc.). All the samples were degassed at 400 °C for 4 h prior to data collection. In the case of uncalcined samples, the samples were preheated at 200 °C to vaporize the physisorbed water molecules. The total pore volume (V_{total}) was taken from the adsorption amount at P/P_0 = 0.99, assuming the complete pore saturation. Specific surface areas were calculated by the BET (Brunauer–Emmett–Teller) method using adsorption data ranging from $P/P_0 = 10^{-3}$–10^{-2}. The micropore volumes (V_{micro}) were calculated by the α_s-plot. Water and toluene adsorption isotherms were obtained using the same apparatus and pretreatment procedures, but measured at 25 °C. Water and toluene (purity >99.5%) were used as adsorbates after purification by

successive freeze-thaw cycles inside the adsorption apparatus. The water and toluene adsorption capacities were reported at $P/P_0 = 0.2$. The determination of the hydrophobicity of solids has been an ambiguous but worthwhile problem for many researchers dealing with solid state and surface chemistry. The determinations have been based so far on water adsorption and porosity measurements under static conditions. In this study, the degree of hydrophobicity, or hydrophobicity index (HI), was defined as the weight ratio of toluene and water adsorbed according to Berke et al. [33]. The corresponding equation can be expressed as $HI = X_{toluene}/X_{water}$, where $X_{toluene}$ and X_{water} represent the weight of toluene and water adsorbed at $P/P_0 = 0.2$ per unit quantity of zeolite, respectively.

Thermal analysis was carried out with differential thermal analysis–thermogravimetry (DTA–TG) (MAC Science Co. Ltd., TG-DTA2000S) from room temperature to 1000 °C at a heating rate of 10 °C/min in a N_2 flow of 50 cm^3/min using α-Al_2O_3 as standard. The acid sites of the zeolite surface were estimated by pyridine adsorption followed by FT-IR spectroscopy. A sample of 20 mg was pressed into a self-supported wafer with a diameter of 20 mm. The wafer was introduced into a Pyrex vacuum IR cell and preheated under vacuum at 400 °C for 2 h. Pyridine was adsorbed at room temperature for 30 min and was then evacuated at 200 °C under vacuum for 1 h to remove physisorbed pyridine molecules [34]. After it was cooled to room temperature, a spectrum was measured in a JASCO FTIR-6100 instrument in transmittance mode. ^{29}Si MAS NMR spectra were taken with a Chemagnetics CMX300 Infinity spectrometer. The ^{29}Si (59.6 MHz) NMR spectra were obtained at a spinning rate of 7 kHz, with recycle delays of 100 s using tetramethylsilane ($Si(CH_3)_4$) as a standard reference and polydimethylsilane as a second reference (−34.4 ppm) relative to tetramethylsilane. All ^{29}Si NMR results were obtained from the 300-MHz instrument.

2.5. Photocatalytic tests

For liquid-phase photocatalytic degradation, photocatalyst (50 mg) and 25 mL of aqueous 2-propanol solution (2.6 mmol/L) were placed to a quartz reaction vessel (50 cm^3). The suspension was magnetically stirred under dark conditions for 2 h to establish adsorption. After being bubbled with oxygen for 30 min under dark conditions, the sample was subsequently irradiated using a 100-W high-pressure Hg lamp (Toshiba SHL-100UVQ-2; light intensity 4 mW/cm^2 at $\lambda = 360$ nm) with magnetic stirring at ambient temperature. Gaseous-phase photocatalytic degradation was carried out using a closed circulating vacuum line equipped with a flat-bottomed quartz cell and a magnetic pumping system (total volume ca. 400 cm^3). After photocatalyst (100 mg) was placed on the quartz cell, air-balanced acetaldehyde gas (ca. 16.2 μmol, 1000 ppm) was charged and was pumped for 2 h until the adsorption equilibrium was reached, and then UV light was irradiated from below using a 200-W high-pressure Hg Xe-lamp (SAN-EI Electric UVF-203S; light intensity 35 mW/cm^2 at $\lambda = 360$ nm) at ambient temperature. In both cases, a portion of the reaction media was collected at appropriate intervals, and residual amounts of organic compounds were quantified using a gas chromatograph (Shimadzu GC-14A) with a flame ionization detector equipped with a Porapak Q column.

3. Results and discussion

3.1. Optimization of dealumination treatment

In a preliminary experiment, dealumination of zeolites was attempted employing HY(5.8) zeolite as a zeolite precursor under a variety of conditions (e.g., different temperatures, acid strengths, and types of acid) in order to optimize the dealumination treatment. Descriptions of the various experiments and the characterization results are tabulated in Table 1.

HY(5.8) zeolite can be dealuminated even under ambient temperature conditions; however, the resulting Al content was 1.80 mmol/g, which corresponds to Si/Al = 8.25. This value is nearly equal to the framework Si/Al ratio of the starting material, 10.3. Upon dealumination, the unit cell shrinks because of shorter Si–O bonds (1.61 Å) replacing longer Al–O bonds (1.75 Å), which is reflected in the peak shift to higher 2θ values in XRD patterns. However, no appreciable change in the lattice constant a_0 was observed in HY(5.8) dealuminated at ambient temperature. These results suggest that framework Al species are hardly expelled in such a condition, in which sufficient hydrophobicity could not be obtained. Aqueous mineral acids are considered to work as efficient hydrolyzing agents for the removal of Al from the framework under reflux conditions.

As the acid concentration increases from 0.1 to 4.0 N, Al content exponentially decreases, which corresponds well to the decrease in lattice constant. Using nitric acid of >1.0 N, SiO_2/Al_2O_3 ratios greater than 100 can be obtained in a single step without significant loss of crystallinity (the crystallinity losses were kept below 20%); meanwhile, single-step dealumination treatments using EDTA or $SiCl_4$ were commonly reported to give a substantial loss in crystallinity, and the resulting hydrophobicity is quite low due to the presence of a vast number of defect sites [23–25]. As previously reported, it can be readily understood that the degree of hydrophobicity is basically related to the residual Al content [35,36]. This can be monitored clearly by pyridine adsorption studies followed by FT-IR spectroscopy. Fig. 1 shows the infrared spectra of pyridine adsorbed onto HY(5.8) zeolites dealuminated with various concentrations of nitric acid. The spectra exhibit all the expected bands assignable to pyridine bound on Brønsted acid sites (1546 cm^{-1}), pyridine bound on Lewis acid sites (1456 and 1621 cm^{-1}), pyridine associated with both Brønsted and Lewis acid sites (1490 cm^{-1}), and hydrogen-bonded pyridine (1446 and 1596 cm^{-1}) [37]. Generally, Brønsted sites attributed to the bridging hydroxyls neighboring the tetrahedrally coordinated Al sites (Scheme 1A) and Lewis acid sites can be assigned to aluminum in defect positions or to extraframework Al species (Scheme 1B and C). Pyridine-adsorbed IR spectra suggest that the untreated HY(5.8) zeolite possesses large amounts of both extraframework and framework Al species (Fig. 1a). As expected, increasing the acid concentration reduces the number of acid sites capable of interacting with the pyridine due to the Al dissolution. In the samples treated with over 0.5 N, two additional bands attributable to surface silanol groups appeared (Fig. 1c–f), proving the creation of silanol groups (Scheme 1D) after the dissolution of the framework Al atoms. Although the sample treated with 1.0 N nitric acid still retains appreciable numbers of Brønsted and Lewis acid sites, most of them disappeared with acid concentrations above 2.0 N (Fig. 1e and f), suggesting the complete removal of Al species from the surface, leaving only silanol nests behind.

Varying the nature of the inorganic acid had little effect on any properties of the resulting material, whereas use of acetic acid was found to be insufficient for the removal of Al from the framework. Highly hydrophobic zeolites with HI > 60 were obtained by using mineral acids of >2.0 N, demonstrating that reduction of Al content below 0.21 mmol/g is essential for attaining high hydrophobicity. Thus, the zeolite hydrophobicity is strongly dependent on the severity of the acid leaching treatment. Dealumination with stronger acidic solutions (over 2.0 N) led to more reduced numbers of Al species; however, complete removal of Al from the crystals by a single step was impossible, and no significant improvement of final HI values was observed. In our methodology, using HY(5.8) as a starting material, 2.0 N nitric acid was found to be sufficient for

Table 1
Textural properties of HY(5.8) zeolites dealuminated under a variety of acid conditions.

Treatment			ICP		XRD		N_2 ads.			H_2O ads. [g] (mg/g)	Toluene ads. [g](mg/g)	HI [g]
Acid	Temp.	Cal temp. (°C)	Global SiO_2/Al_2O_3 ratio [a]	Al content (mmol/g)	a_0 [b] (Å)	Cryst.[c] (%)	S_{BET} [d] (m^2/g)	V_{total} [e] (mL/g)	V_{micro} [f] (mL/g)			
Variation of temperature												
None			5.8 (20.6)	4.27	24.38	100	584	0.404	0.185	43.0	165	3.8
2.0 N HNO_3	R.t.	–	16.5	1.80	24.38	87	703	0.504	0.253	31.0	205	6.6
2.0 N HNO_3	R.t.	1000	16.5	1.80	24.38	106	760	0.578	0.241	16.3	205	12.6
2.0 N HNO_3	Reflux	–	158	0.21	24.35	83	723	0.506	0.256	27.5	197	7.1
2.0 N HNO_3	Reflux	400	158	0.21	24.35	91	777	0.531	0.232	18.8	207	11.0
2.0 N HNO_3	Reflux	600	158	0.21	24.35	95	771	0.530	0.237	7.89	213	27.0
2.0 N HNO_3	Reflux	800	158	0.21	24.34	104	762	0.549	0.240	3.44	209	60.8
2.0 N HNO_3	Reflux	1000	158	0.21	24.34	121	782	0.580	0.244	2.71	208	76.8
Variation of acid concentration												
0.1 N HNO_3	Reflux	1000	10.4	2.70	24.37	85	666	0.544	0.212	30.2	201	6.7
0.5 N HNO_3	Reflux	1000	29.6	1.05	24.35	105	738	0.560	0.240	9.98	208	20.8
1.0 N HNO_3	Reflux	1000	100	0.33	24.35	108	747	0.555	0.245	5.03	211	41.8
4.0 N HNO_3	Reflux	1000	198	0.17	24.33	102	725	0.569	0.241	2.37	194	81.9
Variation of acids												
2.0 N HCl	Reflux	1000	168	0.20	24.34	101	753	0.569	0.247	3.32	201	60.5
2.0 N H_2SO_4	Reflux	1000	178	0.19	24.33	106	759	0.570	0.244	3.05	208	68.2
2.0 N H_3PO_4	Reflux	1000	156	0.21	24.35	112	793	0.604	0.255	3.26	211	64.7
2.0 N acetic acid	Reflux	1000	11.4	2.48	24.37	84	700	0.543	0.238	33.2	197	5.9

[a] Estimated by ICP analysis. Value in parentheses is framework SiO_2/Al_2O_3 ratio determined by ^{29}Si MAS NMR analysis.
[b] Calculated by the equation of $a_0 = d_{100} \times 2/\sqrt{3}$.
[c] Crystallinity based on HY(5.8). Estimated by comparing the sum of peak intensities.
[d] Calculated from the adsorption branch of the N_2 isotherms by the BET (Brunauer–Emmett–Teller) method.
[e] Values at $P/P_0 = 0.99$.
[f] Estimated by α_s-plot.
[g] Values at $P/P_0 = 0.2$.

preparing highly hydrophobic zeolite and was employed as a standard acid reagent for dealumination afterward.

Acid treatment of FAU zeolites with various SiO_2/Al_2O_3 ratios (SiO_2/Al_2O_3 = 13, 36, 54, 92) in the same manner resulted in no notable changes in their microporous structure, whereas zeolites with global SiO_2/Al_2O_3 ratio of lower than 6 were mostly destroyed after the acid treatment. This is due to the rapid dissolution of vast amounts of Al species from the zeolite framework. Although HY(5.8) contains large amount of Al content, its framework Si/Al ratio is estimated to be ca. 10 (Table 1) and the remaining Al species are mostly considered to be an extraframework amorphous aluminum oxide species. This result indicates that the predealuminated Y-zeolites with framework Si/Al ratio higher than 10 are eligible for the acid leaching treatment.

3.2. Structural analysis

The N_2 adsorption–desorption isotherms of the dealuminated Y-zeolites calcined at up to 1000 °C in air are given in Fig. 2, and the structural parameters, together with the adsorption capacities for water and toluene molecules, calculated from the sorption measurements are summarized in Table 1. The N_2 adsorption–desorption isotherms showed typical type I isotherms with a steep increase in the amount of adsorbed N_2 at very low pressures ($P/P_0 < 0.01$) in all samples, proving that the rigid microstructure of the zeolite was retained even after the severe acid and calcination treatments. In all samples, a hysteresis loop closing at $P/P_0 = 0.45$ and a gradual increase in the high-pressure region were observed, reflecting the presence of secondary pores generated during the steaming process. As the calcination temperature increased, the total pore volume slightly increased; the total volume increased from 0.506 to 0.580 cm^3/g when it was calcined at 1000 °C, whereas the micropore volume remained nearly constant. Simultaneously, the BET surface area increased from 723 to 782 m^2/g, in good agreement with the increase in crystallinity estimated from XRD peak intensities (see also Fig. 4 and Table 1). This might be due to meso-order intracrystalline voids created upon calcination being accompanied by reconstruction of the zeolite framework, which will be discussed later.

Additionally, FE-SEM images of $deAl_{1000}$-Y showed octahedral crystals, which are characteristic of FAU zeolite, and neither agglomerated silica particles nor crystals with different morphologies were seen (see Fig. S1). These crystallographic, sorptive, and electrographic characterization results confirm the high structural and thermal stability of the prepared FAU zeolite crystals.

3.3. Adsorption experiments

To estimate the hydrophilic/hydrophobic properties of these series of zeolites, we performed adsorption experiments with two probe molecules of different polarity, water, and toluene. Fig. 3 illustrates the water and toluene adsorption isotherms measured at 25 °C. Adsorption capacities for water and toluene at $P/P_0 = 0.2$ and hydrophobic indices (HI) determined from these values are also listed in Table 1. A lower adsorption capacity in HY(5.8) is due to the presence of large amount of amorphous extraframework Al species, which occlude the micropore channels. As seen in Fig. 3, the adsorbed amount of water markedly decreases as calcination temperature increases, whereas that of toluene remains unchanged. In the low-pressure region, there is a linear increase in the amount of water adsorbed as P/P_0 increases, and the slope of the isotherms decreases as the calcination temperature increases. Surprisingly, the $deAl_{1000}$-Y exhibited extremely low water adsorption in the pressure region $P/P_0 < 0.7$, and adsorption assigned to capillary condensation into micropore channels was observed above $P/P_0 = 0.7$–0.8, indicating extremely weak

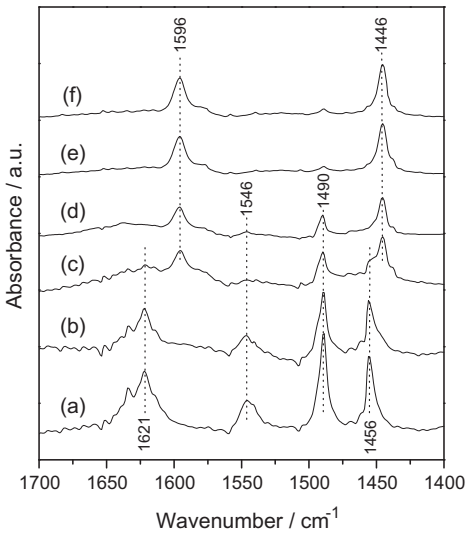

Fig. 1. IR spectra of adsorbed pyridine on (a) HY(5.8) and HY(5.8) dealuminated with aqueous nitric acid solution of (b) 0.1 N, (c) 0.5 N, (d) 1.0 N, (e) 2.0 N, and (f) 4.0 N.

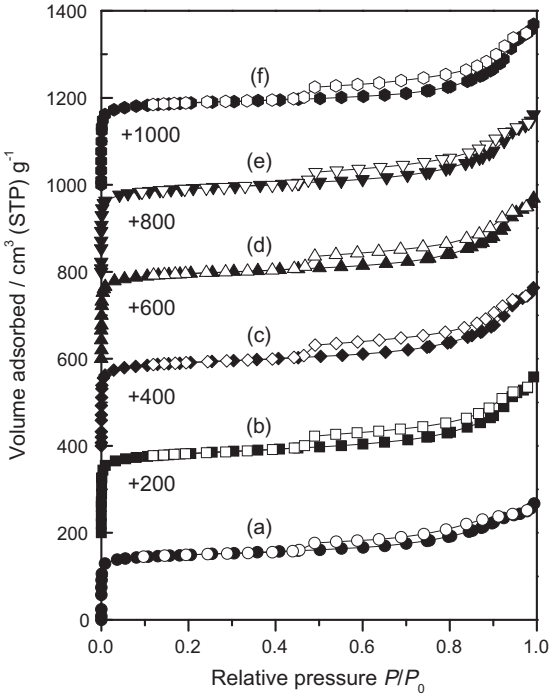

Fig. 2. N_2 adsorption–desorption isotherms of (a) HY(5.8), (b) deAl-Y, and deAl-Y calcined at (c) 400 °C, (d) 600 °C, (e) 800 °C, and (f) 1000 °C in air.

interaction between water molecules and the solid surface, i.e., the strictly hydrophobic nature of the zeolite surface.

For HY(5.8), the HI value increased from 3.8 to 76.8 upon hydrophobization treatment. Higher HI values (HI = 100–130) were attained when predealuminated zeolites, HY(54) and HY(92), were used as starting materials. These values are considerably higher than those of other types of zeolites previously reported elsewhere [35,36,38,39]. Such great enhancement in hydrophobicity was observed neither in uncalcined samples (HI = 7.1) nor in samples directly calcined without dealumination steps (HI = 6.0), proving that both dealumination and subsequent calcination steps are essential for achieving high hydrophobicity. It is noteworthy that the hydrophobicity of thus-prepared Y-zeolite was far superior to that of silicalite-1 (HI = 30.0 for the samples calcined at 1000 °C), a siliceous zeolite with MFI topology generally recognized as highly hydrophobic. More interestingly, thus-prepared Y-zeolite is as hydrophobic as siliceous Y-zeolite (USY; SiO_2/Al_2O_3 = 810, Al content <0.04 mmol/g) calcined at the same temperature (HI = 102), whereas it still contains an appreciable amount of aluminum (ca. 0.21 mmol/g) in its crystal structure. Considering the results of pyridine-adsorbed FT-IR measurement, this might be due to the selective removal of Al species from the zeolite surface, i.e., the remaining Al species appear to be present in intraplanar sites of zeolite crystal, to which acids and pyridine molecules are inaccessible.

Fig. 4 shows the HI values plotted as a function of the calcination temperatures. A clear correlation can be confirmed between HI values and calcination temperatures, demonstrating that the hydrophobic character of Y-zeolite could be improved during the calcination treatment. In the case of basic aluminosilicate zeolites, it has been commonly known that the Al sites and related cation sites work as strong adsorption sites of polar molecules via electrostatic or dipolar–dipolar interactions [15,16]; therefore, the specific interactions can be reduced by dealumination and decationization or chemical treatments using organosilane coupling agents [40–42]. However, high hydrophobicity, as above, could not be obtained by dealumination treatment alone, suggesting that the silanol defect sites created during the acid treatment still act as strong adsorption sites. It can be speculated from the slight increase in surface area and total pore volume at the elevated temperature that the calcination step provokes rearrangement of the framework structure and the great improvement in hydrophobicity is derived from the formation of refined silica surface with fewer adsorption sites.

3.4. Hydrophobization mechanism

The change in the number of silanol groups of the dealuminated zeolites during the calcination treatment can be tracked by thermogravimetric analysis. TG curves and the first derivatives of HY(5.8) before and after the acid treatment are shown in Fig. 5. Weight losses observed at $T < 100$ °C correspond to desorption of physisorbed water molecules. The dealuminated HY(5.8) shows additional weight loss at $T > 100$ °C with several broad peaks in its first derivative, which are attributable to dehydroxylation

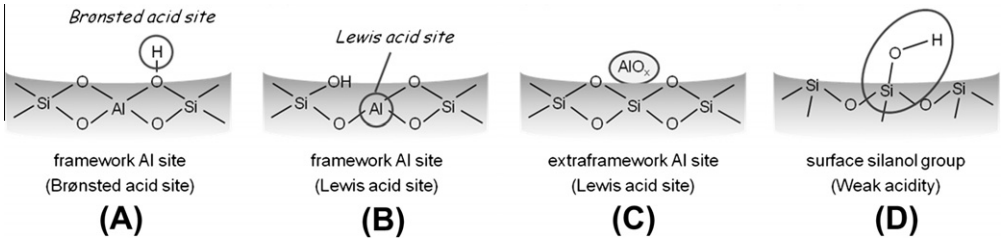

Scheme 1. Schematic illustrations of adsorption sites on zeolite surface.

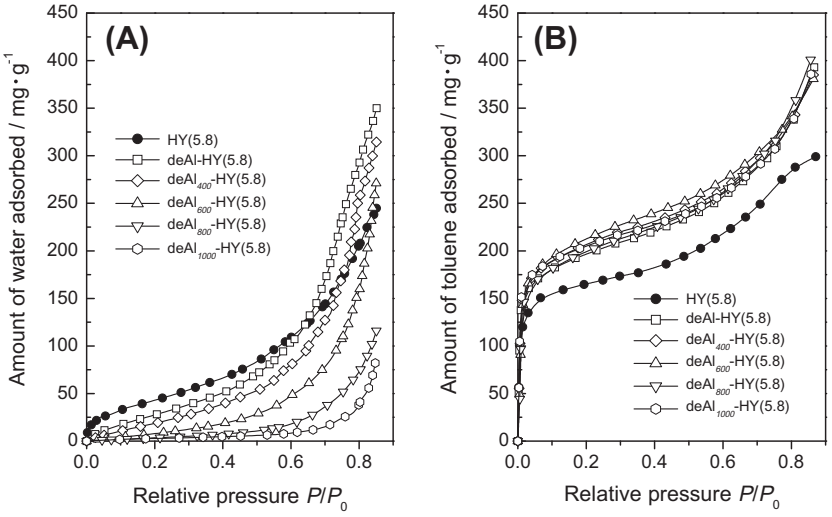

Fig. 3. (A) Water and (B) toluene adsorption isotherms of HY(5.8), deAl-Y, and deAl-Y calcined at different temperatures (400–1000 °C) measured at 25 °C.

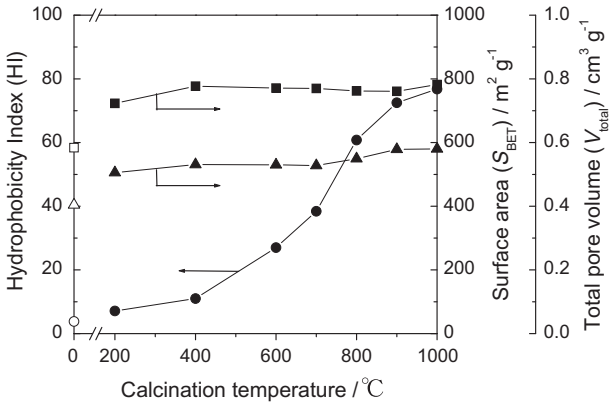

Fig. 4. Change in the hydrophobicity index (●, HI), surface area (■, S_{BET}), and total pore volume (▲, V_{total}) of deAl-Y as a function of calcination temperature (open symbols correspond to HY(5.8) zeolite precursor).

condensation of silanol groups, most of which occurred in the range of 100–700 °C (corresponding to 2.36 wt.% weight loss). This clearly suggests that the improvement in hydrophobicity arises from the removal of the silanol groups, as deduced above. Indeed, deAl$_{700}$-Y exhibited an improved hydrophobic character compared to the uncalcined sample; however, the calcination at 700–1000 °C (corresponding to 0.23 wt.% loss) led to a further improvement in hydrophobicity, suggesting that further dehydroxylation to create more a refined silica surface is still ongoing above 700 °C.

FT-IR and ^{29}Si MAS NMR spectroscopy provide more clear evidence for the dehydroxylation of silanols within zeolite crystals. The FT-IR spectrum of deAl-Y clearly showed a broad band at around 954 cm^{-1} due to a large concentration of Si–OH defect groups present in the sample, and the intensity of this band gradually decreased upon calcination at elevated temperatures, elucidating the idea we suggested above (see Fig. S2). Further, ^{29}Si MAS NMR spectra of dealuminated HY(5.8) and deAl-Y calcined at different temperatures are given in Fig. 6, which exhibits three different components centered at −101, −107, and −111 ppm. Pérez-Pariente et al. reported that the line at −107 ppm with high intensity corresponds to Si atoms surrounded by 4 Si atoms and an additional line positioned at −111 ppm would correspond to nonequivalent silicon atoms, with 4 Si atoms in the second coordination sphere, occupying different crystallographic sites from that at −107 ppm [43]. The deAl-Y exhibited a broad band at −101 ppm that is attributable to the superposition of Si (3Si, 1OH) components. The intensity of this resonance line apparently decreased the calcination at higher temperatures, proving the healing of silanol groups and being well consistent with the results of FT-IR spectra. Similarly, a decrease in the intensity of the −111 ppm resonance line was observed, probably reflecting the realignment of the silica network. This simultaneous healing of the zeolite framework can be well understood, provided that the nonequivalent silicon atoms are the ones sterically distorted by the silanol groups present in the vicinity. In the spectrum of deAl$_{1000}$-Y, only a single line assignable to the Si (4Si) resonance was observed, representing the formation of a highly sophisticated silica network (Fig. 6e).

Another question that needs to be addressed is the mechanism of healing defect silanol sites. To attain such a refined silica network as evidenced by ^{29}Si MAS NMR, the silanol nests left behind after the Al dissolution should be occupied by Si atoms. To ascertain the healing mechanism and to examine the possibility of filling the defect sites by adding some silicon sources, independent experiments were carried out. However, the addition of tetraethoxyorthosilicate (TEOS) and silicon tetrachloride ($SiCl_4$) during the acid treatment had no effect on the hydrophobicity of the resulting materials. This result indicates that under our experimental conditions the hydrophobization of zeolites can be accomplished only by the thermal dehydroxylation condensation of silanols.

The silanols in the zeolitic crystals can be classified into three groups: (i) adjacent silanols hydrogen-bonded with each other (e.g., silanol nests), (ii) isolated silanols, and (iii) terminal framework silanols. It is believed that the silanol groups located at different crystallographic positions exhibit different dehydroxylation behavior during calcination, which might be reflected in the TG curves. It has commonly been reported that the adjacent silanol groups forming silanol nests readily condense each other by dehydroxylation at 100–600 °C, forming siloxane bonding, and thus part of the defect silanol sites can be removed [29,44]. However, this cannot provide any consistent interpretation for the removal of isolated or terminal silanol groups. Another plausible explanation for healing defect silanol sites is a T-jump mechanism whereby defect sites migrate from the internal portion to the outer surface of the crystal [22]. Considering the dehydroxylation behavior observed in TG and ^{29}Si MAS NMR, it is reasonable to hypothesize that the defect silanol groups can be healed via a following

mechanism. Adjacent silanol groups, including silanol nests, can be readily healed at below 700 °C through dehydroxylation condensation; in contrast, part of discrete silanols are likely to be healed at above 700 °C being accompanied by the migration of the silanol groups, although a certain number of terminal silanols in the external surface are scarcely removed by thermal treatment.

3.5. Effect of structure type of zeolite

To show the generality of this methodology, in this part, topologically different zeolites were treated in the same manner as described above.

The XRD patterns and water/toluene adsorption isotherms of various zeolites before and after the treatment are shown in Figs. 7 and 8, respectively, and the textural properties obtained by chemical and sorptive analyses are summarized in Table 2. As shown in Fig. 7, in all zeolite types, appreciable increases in diffraction peak intensities were observed in low-angle region after the hydrophobization treatment. This is due to the rearrangement of the microporous structures during the calcination treatment, as discussed above.

The water and toluene adsorption isotherms before the hydrophobization treatment are both of type I according to the IUPAC classification, which is characteristic of microporous solids. In contrast, all zeolite samples after the treatment exhibited quite different behavior in water adsorption, which is of type III, while still exhibiting type I isotherms in toluene adsorption. Using H-MOR(15.4) as a starting material resulted in a major collapse of the zeolite microstructure when it was calcined at 1000 °C, while it had been mostly maintained up to 800 °C. This thermal instability is probably due to the high Al content remaining in the acid-treated sample (SiO_2/Al_2O_3 = 22.4).

For H-ZSM-5(38), which is a middle-pore zeolite with a 10-membered ring, Al species were scarcely expelled from the framework, resulting in a slight increase in hydrophobicity (HI: 1.7 → 10.9). This is conceivably because of the rigidity of the framework derived from their crystalline structures, or otherwise, because of their narrower channel sizes. In the case of MOR and ZSM-5 zeolites, a careful acid treatment using a stronger acid solution would be required to obtain sufficiently dealuminated zeolites [29]. A significant improvement in hydrophobicity was observed only in H-Beta(20) without significant loss of its crystallinity, probably because of its porous structure, similar to that of FAU zeolite (both possess three-dimensional channel systems with 12-membered rings). However, the resulting HI value, 26.5, was not as high as that of HY(5.8) under the preparation conditions examined in this study. We presume that the main differences in the degree of

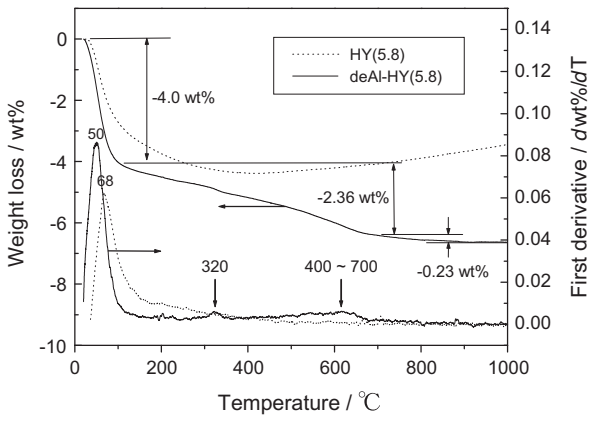

Fig. 5. Thermal analysis of HY(5.8) (dotted curves) and deAl-Y (solid curves).

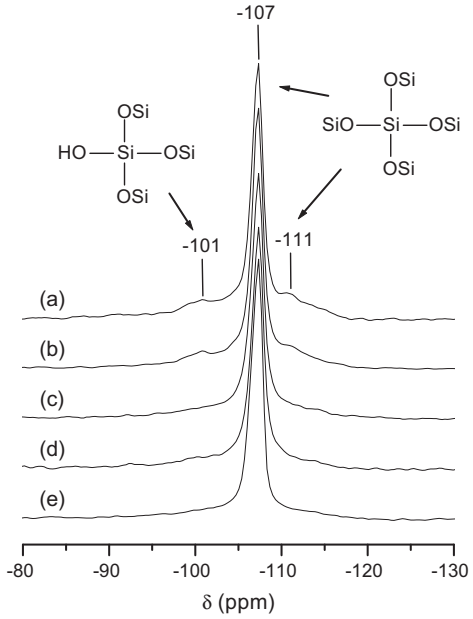

Fig. 6. ^{29}Si MAS NMR spectra of (a) deAl-Y and deAl-Y calcined at (b) 400 °C, (c) 600 °C, (d) 800 °C, and (e) 1000 °C.

hydrophobicity are essentially related to the different crystalline structures, which will determine the feasibility of dealumination and/or dehydroxylation of defect silanol groups, and cannot be solely attributed to initial SiO_2/Al_2O_3 ratios. These comparative studies based on hydrophobicity index have indicated that the hydrophobicity of thus-prepared FAU zeolite would be the highest among other structural types of zeolites. For attaining high hydrophobicity of other structural types of zeolites, extensive exploration of optimum preparation conditions would be required.

3.6. Application of hydrophobic FAU zeolite as a host material for TiO_2

Our method demonstrated here can afford prominent hydrophobicity of zeolite via facile preparation steps without any significant loss in porosity and without addition of any extra silicon sources. Further, the material remains highly crystalline and thermally stable.

Hydrophobic zeolites can be regarded as ideal host materials for encapsulating nanosize metal, metal oxide, and organic supermolecular catalyst species because of the defined geometry of the cavities and channels of nanometer length, their high chemical and thermal stability, and their improved adsorption properties for organic molecules [45,46]. Furthermore, zeolites potentially have additional advantages as hosts for photocatalysts, such as photochemical stability and transparency to UV–visible light irradiation [47]. These unique features have led to a number of studies on the encapsulation of TiO_2 species into zeolites [48–50]. To demonstrate the availability of thus-prepared hydrophobic Y-zeolite as a support for TiO_2, we examined photocatalytic activity of zeolite-supported TiO_2 using photocatalytic degradation of 2-propanol diluted in water and acetaldehyde diluted in air under UV light irradiation as model reactions.

To ascertain the effect of zeolite hydrophobicity on photocatalysis, 10 wt.% of TiO_2 was systematically loaded onto $deAl_{1000}$-Y as well as zeolites with various SiO_2/Al_2O_3 ratios (SiO_2/Al_2O_3 = 5.8, 36, 54, 92, and 810). XRD patterns and N_2 adsorption isotherms (XRD patterns are shown in Fig. S3; textural parameters obtained from N_2 adsorption isotherms are summarized in Table 3) confirmed that the zeolite microstructures still remained even after

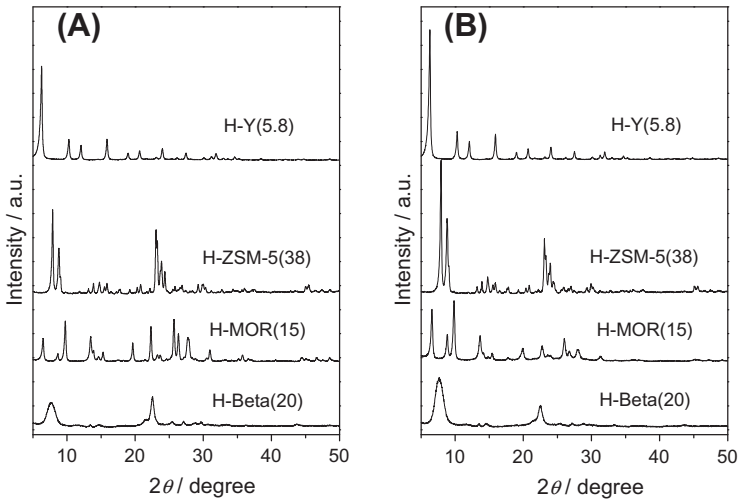

Fig. 7. X-ray diffraction patterns of HY (SiO_2/Al_2O_3 = 5.8), H-ZSM-5 (SiO_2/Al_2O_3 = 38), H-MOR (SiO_2/Al_2O_3 = 15.4), and H-Beta (SiO_2/Al_2O_3 = 20) zeolites (A) before and (B) after the hydrophobization treatment, which was performed using 2.0 N nitric acid solution under reflux conditions, followed by calcination at 1000 °C in air (calcined at 800 °C for H-MOR).

the TiO_2 loading. Slight peaks assignable to the (1 0 1) diffraction plane of anatase TiO_2 crystals observed at $2\theta = 25.4°$ in XRD patterns indicated the formation of anatase TiO_2 clusters. All samples still retained their large surface areas and pore volumes available enough as adsorbents, although they decreased by 5–12% and 8–20%, respectively, after the TiO_2 loading due to the occlusion of micropores by the TiO_2 clusters. In the case of $deAl_{1000}$-Y, the mean surface area decreased from 782 to 705 m^2/g, and the total pore volume decreased from 0.580 to 0.477 cm^3/g after the 10 wt.% TiO_2 loading. As shown in Table 3, sorptive analyses using water and toluene as adsorbates confirmed different hydrophobic/organophilic character of the zeolite supports. The HI value increased fundamentally as the SiO_2/Al_2O_3 ratio increases (all HI values are of zeolite samples calcined at 1000 °C in air).

Fig. 9 shows reaction time profiles of the photocatalytic degradation of 2-propanol diluted in water using TiO_2 photocatalysts supported on zeolites with various SiO_2/Al_2O_3 ratios. The adsorption of 2-propanol mostly took place within 2 h, and the loss of 2-propanol during the bubbling was negligible. The amount of 2-propanol adsorbed in 2 h was found to be independent of the hydrophobicity of zeolites. This is because adsorption capacity fundamentally depends on the total pore volume (V_{total}) available for accommodation. After UV light irradiation, 2-propanol was photocatalytically decomposed into H_2O and CO_2, via acetone and acetaldehyde as intermediate products, according to pseudo-first-order kinetics. As can be seen from Table 3, TiO_2 photocatalysts supported on hydrophilic zeolites (SiO_2/Al_2O_3 = 5.8–54, which corresponds to HI < 10) are rather less photoactive than TiO_2 powder (P-25); however, noticeable improvements in degradation rates were observed by utilizing hydrophobic zeolite supports. Surprisingly, $TiO_2/deAl_{1000}$-Y (SiO_2/Al_2O_3 = 158) afforded a high degradation rate, k = 10.1, which was ca. 10 times higher than that of TiO_2/HY(5.8) (k = 0.95). This noticeable improvement in photoactivity is due to the high affinity with organic molecules evidenced by the sorptive analyses, that is, the hydrophobic zeolite surface with fewer adsorption sites provides organic molecules with high diffusibility within the micropore channels and high accessibility to the TiO_2 active sites, resulting in higher photocatalytic activity. The photocatalytic activity of $TiO_2/deAl_{1000}$-Y was yet lower than that of TiO_2 supported on highly siliceous Y-zeolite (TiO_2/HY(810)) simply because of lower HI value (HI = 76.8) than that of HY(810) (HI = 102); however, the easy preparation steps of $deAl_{1000}$-Y demonstrated in this study are believed to be beneficial for simplifying the manufacturing process and reducing the amount of waste water, because synthesis of highly siliceous Y-zeolite requires repeated acid treatment or use of strong mineral acids. It is also worth mentioning that the photoactivity of the physical mixture of anatase TiO_2 (ST-01) and $deAl_{1000}$-Y-zeolite (k = 3.66) was considerably lower than that of $TiO_2/deAl_{1000}$-Y composite photocatalyst (k = 10.1) and was similar to that of parent TiO_2 (k = 3.69), implying that the proximity of TiO_2 photoactive sites and adsorption sites plays a crucial role in photocatalysis in water.

A similar tendency was observed in the photocatalytic degradation of acetaldehyde diluted in air. Fig. 10 compares some reaction time profiles of the TiO_2 photocatalysts supported on various zeolites. The zeolite-supported TiO_2 photocatalysts exhibited different adsorption rates for acetaldehyde gas depending on the hydrophilic/hydrophobic nature of their zeolite supports before UV light irradiation, where higher adsorption rates were attained on more hydrophobic zeolites. The apparent photocatalytic degradation rate of TiO_2 was significantly improved by the combination with zeolite supports (Table 3), and in particular, use of highly hydrophobic zeolites, such as $deAl_{1000}$-Y and HY(810), as supports allowed efficient elimination of low-concentration acetaldehyde gas. The use of $deAl_{1000}$-Y resulted in markedly faster adsorption of acetaldehyde gas and higher degradation rates (k = 13.3), which are as high as that of HY(810), compared with the case of hydrophilic zeolites (k = 7.51 for HY(5.8)). Unlike the case of aqueous phase reaction, the physically mixed sample showed adsorption and degradation rates similar to those of $TiO_2/deAl_{1000}$-Y in the gas phase reaction. This might be simply because of higher diffusibility of organic molecules in air than in water, i.e., volatile organic compounds once adsorbed on zeolite surface can easily migrate from zeolite crystals to TiO_2 particles.

To gain further precise insight into the effect of zeolite hydrophobicity on the TiO_2 degradation efficiency, degradation rate constants determined by the above two photocatalytic tests were plotted against the HI values of the zeolite supports (Fig. 11). In zeolite-supported TiO_2 systems, good linear correlations were observed between the rate constants and HI values determined based on the sorptive analyses, whereas other structural parameters of zeolites, such as remaining surface area and pore volume, did not provide such a distinct correlation. Furthermore, there was no

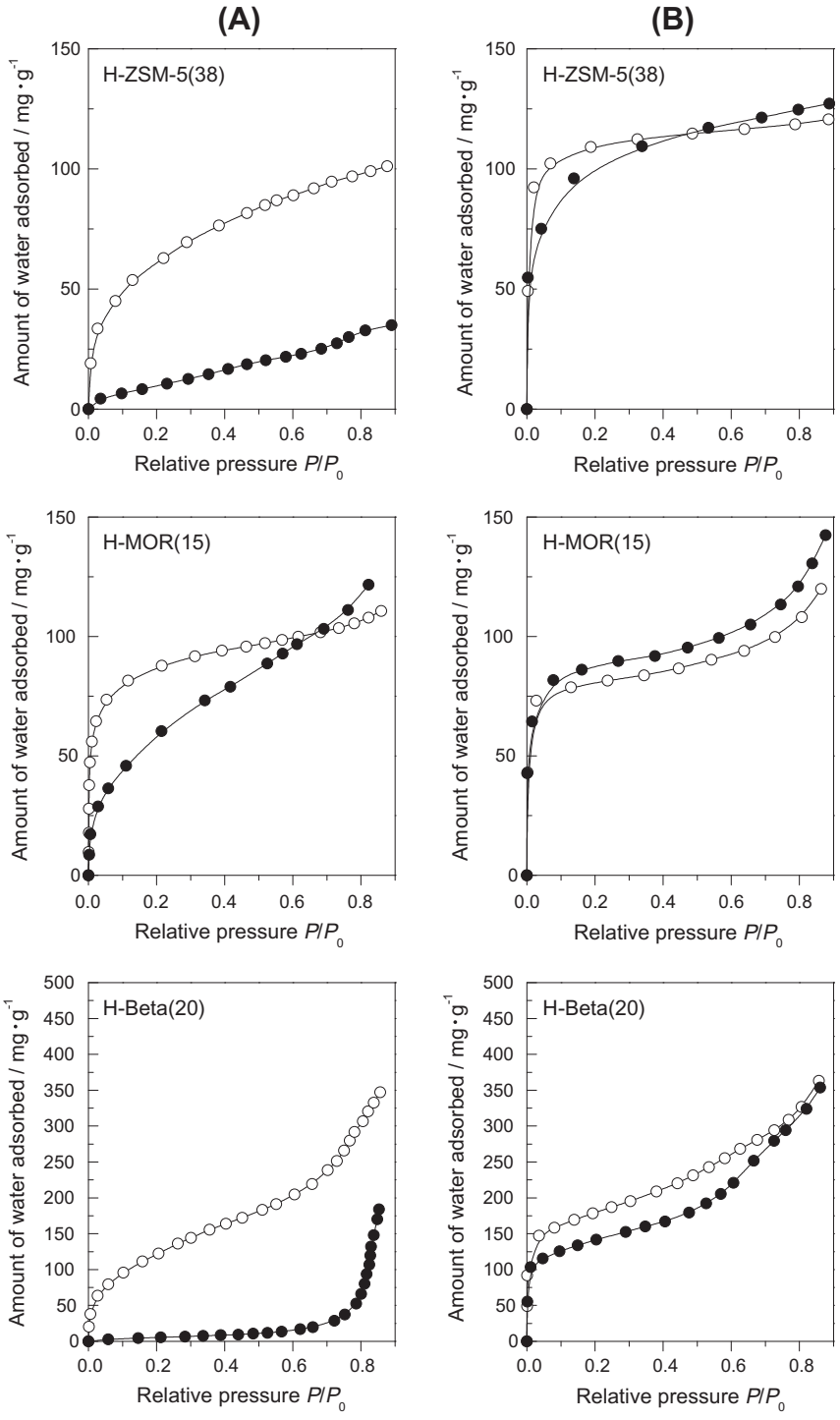

Fig. 8. (A) Water adsorption isotherms and (B) toluene adsorption isotherms of H-ZSM-5(38), H-MOR(15), and H-Beta(20) zeolites before (○, open circle) and after (●, filled circles) the hydrophobization treatment, which was performed using 2.0 N nitric acid solution under reflux conditions, followed by calcination at 1000 °C in air (calcined at 800 °C for H-MOR).

significant difference in the crystallinity, average particle size, and dispersibility of TiO_2 particles among the samples we examined; the TEM images showed uniformly dispersed nanosize TiO_2 particles whose average particle size slightly increased as the hydrophobicity of the zeolite support improved (the average particle size was estimated to be 2.5 nm in TiO_2/HY(5.8) and 4.0 nm in TiO_2/deAl$_{1000}$-Y (see Fig. S4)), being reflected in the slightly increased intensity of the diffraction peaks corresponding to anatase TiO_2 crystals, as seen in Fig. S3. There might be a possibility that these structural factors of TiO_2 particles affect the reaction rates; however, no clear correlations were identified between the rate constant and such factors, because of very small changes and broad distributions of the particle size. It is believed that they make much smaller contributions to the photocatalytic activity than the effect of hydrophobicity of the zeolite support unless the TiO_2 content is extensively varied. For more detailed

Table 2
Textural properties of various types of zeolites before and after the hydrophobization treatment.

Sample	Treatment		ICP		N_2 ads.			H_2O ads. [e] (mg/g)	Toluene ads. [e] (mg/g)	HI [e]	Remarks
	Acid	Cal temp. (°C)	Global SiO_2/Al_2O_3 ratio [a]	Al content (mmol/g)	S_{BET} [b] (m^2/g)	V_{total} [c] (mL/g)	V_{micro} [d] (mL/g)				
HY(5.8)	None		5.8 (20.6)	4.27	584	0.404	0.185	43.0	165	3.8	FAU (3D with 12-ring)
	2 N HNO_3	1000	158	0.21	782	0.580	0.244	2.71	208	76.8	Highly hydrophobic
H-ZSM-5(38)	None		38	0.83	411	0.196	0.186	64.7	109	1.7	MFI (3D with 10-ring)
	2 N HNO_3	1000	42	0.76	385	0.179	0.134	9.62	105	10.9	Slightly dealuminated
H-MOR(15)	None		15.4	1.91	452	0.211	0.178	86.5	80.5	0.9	MOR (1D with 12-ring)
	2 N HNO_3	800 [f]	22.4	1.36	510	0.272	0.190	57.9	87.3	1.5	Slightly dealuminated
H-Beta(20)	None		20	1.55	605	0.632	0.166	121	179	1.5	BEA (3D with 12-ring)
	2 N HNO_3	1000	78	0.42	501	0.674	0.147	5.31	141	26.5	Hydrophobic

[a] Value in parentheses is framework SiO_2/Al_2O_3 ratio determined by ^{29}Si MAS NMR analysis.
[b] Calculated from the adsorption branch of the N_2 isotherms by BET (Brunauer–Emmett–Teller) method.
[c] Values at $P/P_0 = 0.99$.
[d] Estimated by α_s-plot.
[e] Values at $P/P_0 = 0.2$.
[f] Calcined at 800 °C due to thermal instability. Calcination at 1000 °C led to major collapse of the microporous structure.

Table 3
Textural properties of zeolite-supported TiO_2 photocatalysts and their first-order rate constants in the photocatalytic degradation of 2-propanol diluted in water and acetaldehyde diluted in air.

Catalyst	Global SiO_2/Al_2O_3 ratio[a]	N_2 ads.		HI of zeolite[d]	First-order rate constant, k (10^{-3} min^{-1})[e]	
		S_{BET}[b] (m^2/g)	V_{total} [c] (mL/g)		2-Propanol in water (2.6 mmol/L)	Acetaldehyde in air (1000 ppm)
TiO_2/HY(5.8)	5.8	551	0.363	6.0	0.95	7.51
TiO_2/HY(36)	36	684	0.428	30.4	1.33	7.14
TiO_2/HY(54)	54	751	0.466	40.3	3.09	8.20
TiO_2/HY(92)	92	740	0.463	46.9	4.73	9.63
TiO_2/HY(810)	810	750	0.457	102	15.4	13.3
TiO_2/$deAl_{1000}$-Y	158	705	0.477	76.8	10.1	13.3
TiO_2 (ST-01) + $deAl_{1000}$-Y[f]	158	731	0.582	76.8	3.66	13.1
TiO_2 (P-25)	–	51.7	ND	ND	3.69	1.44
TiO_2 (ST-01)	–	271	ND	ND	2.70	0.95

[a] Determined by ICP analysis.
[b] Calculated from the adsorption branch of the N_2 isotherms by BET (Brunauer–Emmett–Teller) method.
[c] Values at $P/P_0 = 0.99$.
[d] Values after calcination at 1000 °C in air. Determined from adsorbed amounts of water and toluene at $P/P_0 = 0.2$.
[e] On a TiO_2 mass base.
[f] Physical mixture of anatase TiO_2 powder (ST-01) and $deAl_{1000}$-Y with a mass ratio of 10:90. ND = not determined.

understanding of zeolite-supported TiO_2 photocatalysts, readers are referred to other literature that has studied several structural factors of TiO_2 affecting the photocatalytic activity [51].

The distinct correlation between the rate constants and HI values shown here unambiguously indicates that the hydrophobicity of zeolite surely plays a dominant role in determining the photocatalytic activity in both liquid- and gaseous-phase photocatalytic reactions. A deviation of TiO_2/HY(5.8) from the linear correlation can be explained by the fact that HY(5.8) includes a significant amount of extraframework Al species, which create strong adsorption sites for polar molecules inside the micropore cavities, as mentioned. The liquid phase reaction provided a linear correlation with a steeper slope than the gaseous phase reaction, indicating that hydrophobicity of zeolite plays a more dominant role in the liquid phase reaction than in the gaseous phase reaction. A plausible explanation for this is the effect of water molecules. As evidenced by the sorptive analyses, water molecules can be more readily transferred inside the micropore channels of hydrophilic zeolites due to the presence of a large number of adsorption sites compared with hydrophobic zeolites. In the case of liquid phase reactions where water molecules are present as a majority in the reaction solution, adsorption of water competes with that of organic molecules and frequently retards the mass transfer of organics, and thus, the adsorption kinetics of water significantly affects the photocatalytic efficiency.

These results practically revealed that highly hydrophobic Y-zeolite significantly improves the photocatalytic efficiency of TiO_2 photocatalysts. In addition, the prepared photocatalyst could be separated easily from the reaction solution by simple filtration and could be used repeatedly without appreciable loss of catalyst weight and photocatalytic degradation rate, which may simplify the recovery of the photocatalyst from the treated water and may make the handling of the TiO_2 photocatalyst easier. Thus, the hydrophobic Y-zeolite prepared in our methodology can be envisaged as a potent support for the TiO_2 photocatalyst, especially suited to adsorb and condense organic substrates diluted in water and air, owing to its improved hydrophobicity.

4. Conclusions

Highly hydrophobic FAU zeolite was prepared without significant loss of crystallinity and sorption capacity by an easy two-step preparation method, which consists of predealumination treatment using mineral acids and subsequent calcination treatment at elevated temperature. A distinct correlation was found between the hydrophobicity and the calcination temperatures, and calcination at a higher temperature led to a more hydrophobic nature of the zeolites. The thermogravimetric, IR, and NMR analyses confirmed that high hydrophobicity can be attained by the formation of a refined silica surface having fewer adsorption sites, which is

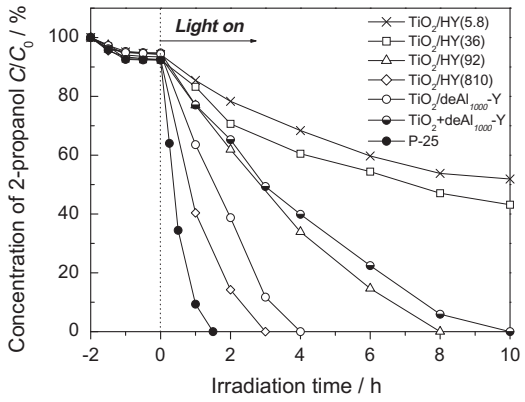

Fig. 9. Time course of concentration of 2-propanol in photocatalytic degradation using TiO_2 photocatalysts supported on various Y-zeolites. Reaction conditions: initial concentration of 2-propanol solution = 2.6 mmol/L, catalyst amount = 2 g/L, room temperature.

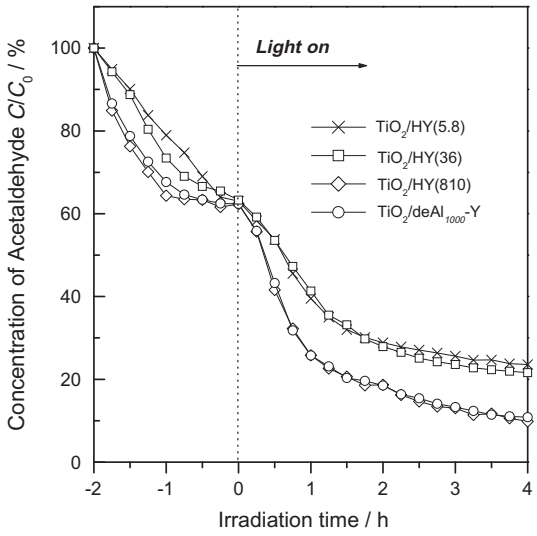

Fig. 10. Time course of concentration of acetaldehyde in photocatalytic degradation using TiO_2 photocatalysts supported on various Y-zeolites. Reaction conditions: initial concentration of acetaldehyde gas = 1000 ppm in air, catalyst amount = 0.25 g/dm^3, room temperature.

accompanied by a healing of the silanol defect sites through dehydroxylation condensation. The resulting FAU zeolites were highly crystalline and structurally and thermally stable and are highly hydrophobic compared to the other structural types of zeolites. When thus-prepared hydrophobic FAU zeolite was utilized as a support for TiO_2 photocatalyst, the photocatalytic degradation rates were significantly improved both in aqueous- and in gaseous phase reactions because of its improved hydrophobic character, which was clearly elucidated on the basis of sorptive analyses and photocatalytic tests. It was also practically demonstrated that the photocatalytic efficiency of zeolite-supported TiO_2 is strongly associated with the surface hydrophobicity of zeolite and the corresponding adsorption kinetics of water and organic molecules.

We expect that this preparation route will be extendable to the other types of zeolite materials by optimizing the preparation conditions, although the highest hydrophobicity was observed in FAU zeolite. Due to their prominent hydrophobicity, they could advantageously replace conventional molecular sieves, adsorbents, and catalyst supports in the specific applications that require a high affinity with organic molecules. In particular, the combination of

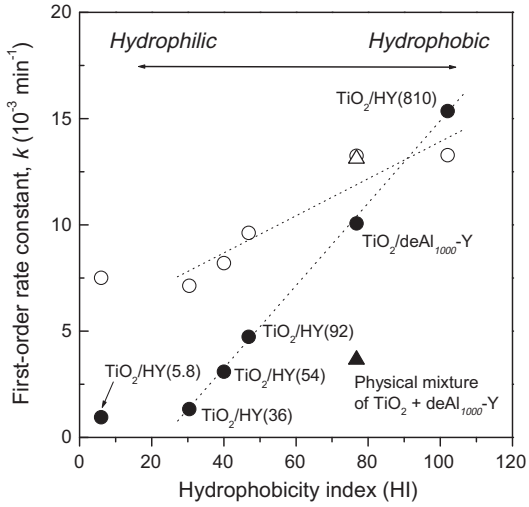

Fig. 11. Correlation between rate constant in photocatalytic degradation k and hydrophobicity index (HI) of zeolite supports (filled circles: degradation of 2-propanol diluted in water; open circles: degradation of acetaldehyde diluted in air; triangle symbols correspond to the physically mixed sample).

a TiO_2 photocatalyst with the hydrophobic FAU zeolites is expected to greatly assist photocatalytic degradation reactions involving organic molecules and will expand the application of TiO_2 photocatalysts for environmental remediation.

Acknowledgments

The present work was supported by Grants-in-Aid for Scientific Research (KAKENHI) from the Ministry of Education, Culture, Sports, Science and Technology (Nos. 20360363 and 21656207). Y.K. thanks the JSPS Research Fellowships for Young Scientists for support.

Appendix A. Supplementary material

Supplementary data associated with this article can be found, in the online version, at doi:10.1016/j.jcat.2011.09.031.

References

[1] A. Fujishima, K. Honda, Nature 238 (1972) 37.
[2] A. Fujishima, T.N. Rao, D.A. Tryk, J. Photochem. Photobiol. C 1 (2000) 1.
[3] M.R. Hoffmann, S.T. Martin, W. Choi, D.W. Bahnemann, Chem. Rev. 95 (1995) 69.
[4] A.L. Linsebigler, G. Lu, J.T. Yates, Chem. Rev. 95 (1995) 735.
[5] H. Yamashita, M. Anpo, Curr. Opin. Solid State Mater. Sci. 7 (2003) 471.
[6] H. Yamashita, S. Kawasaki, S. Yuan, K. Maekawa, M. Anpo, M. Matsumura, Catal. Today 126 (2007) 375.
[7] H. Yamashita, K. Mori, S. Shironita, Y. Horiuchi, Catal. Surv. Asia 12 (2008) 88.
[8] J. Zhang, T. Ayusawa, M. Minagawa, K. Kinugawa, H. Yamashita, M. Matsuoka, M. Anpo, J. Catal. 198 (2001) 1.
[9] Y.H. Hsien, C.F. Chang, Y.H. Chen, S. Cheng, Appl. Catal. B 31 (2001) 241.
[10] Y. Kuwahara, H. Yamashita, J. Mater. Chem. 21 (2011) 2407.
[11] Y. Kuwahara, T. Kamegawa, K. Mori, H. Yamashita, Curr. Org. Chem. 14 (2010) 616.
[12] N.Y. Chen, J. Phys. Chem. 80 (1976) 60.
[13] E.M. Flanigen, J.M. Bennet, R.W. Grose, J.P. Comen, R.L. Patton, R.M. Kirschner, J.V. Smith, Nature 271 (1978) 512.
[14] H. Stach, U. Lohse, H. Thamm, W. Schirmer, Zeolites 6 (1986) 74.
[15] K. Tsutsumi, K. Mizoe, Colloids Surf. 37 (1989) 29.
[16] T. Kawai, K. Tsutsumi, Colloid Polym. Sci. 270 (1992) 711.
[17] G. Engelhardt, U. Lohse, V. Patzelová, M. Mägi, E. Lippmaa, Zeolites 3 (1983) 233.
[18] T.H. Fleisch, B.L. Meyers, G.J. Ray, J.B. Hall, C.L. Marshall, J. Catal. 99 (1986) 117.
[19] R.A. Beyerlein, G.B. McVicker, L.N. Yacullo, J.J. Ziemiak, J. Phys. Chem. 92 (1988) 1967.
[20] A. Gola, B. Rebours, E. Milazzo, J. Lynch, E. Benazzi, S. Lacombe, L. Delevoye, C. Fernandez, Micropor. Mesopor. Mater. 40 (2000) 73.

[21] E.F.T. Lee, L.V.C. Rees, J. Chem. Soc. Faraday Trans. 83 (1987) 1531.
[22] C.W. Jones, S.J. Hwang, T. Okubo, M.E. Davis, Chem. Mater. 13 (2001) 1041.
[23] G.T. Kerr, J. Phys. Chem. 72 (1968) 2594.
[24] G.T. Kerr, J. Phys. Chem. 73 (1969) 2780.
[25] M.W. Anderson, J. Klinowski, Zeolites 6 (1986) 455.
[26] F. Lónyi, J.H. Lunsford, J. Catal. 136 (1992) 566.
[27] W. Hölderich, M. Hesse, F. Näumann, Angew. Chem. Int. Ed. 27 (1988) 226.
[28] E.B. Lami, F. Fajula, D. Anglerot, T.D. Courieres, Micropor. Mater. 1 (1993) 237.
[29] P. Wu, T. Komatsu, T. Yashima, J. Phys. Chem. 99 (1995) 10923.
[30] C.S. Cundy, P.A. Cox, Chem. Rev. 103 (2003) 663.
[31] E. Dempsey, G.H. Kuhl, D.H. Olson, J. Phys. Chem. 73 (1969) 387.
[32] H. Lechert, Zeolites 17 (1996) 473.
[33] C.H. Berke, A. Kiss, P. Kleinschmit, J. Weitkamp, Chem. Eng. Technol. 63 (1991) 623.
[34] E. Selli, L. Forni, Micropor. Mesopor. Mater. 31 (1999) 129.
[35] I. Batonneau-gener, A. Yonli, S. Hazael-pascal, J.P. Marques, J.M. Lopes, M. Guisnet, F.R. Ribeiro, S. Mignard, Micropor. Mesopor. Mater. 110 (2008) 480.
[36] I. Halasz, M. Agarwal, B. Marcus, W.E. Cormier, Micropor. Mesopor. Mater. 84 (2005) 318.
[37] T.R. Hughes, H.M. White, J. Phys. Chem. 71 (1967) 2192.
[38] A.H. Yonli, I. Gener, S. Mignard, Micropor. Mesopor. Mater. 132 (2010) 37.
[39] J. Stelzer, M. Paulus, M. Hunger, J. Weitkamp, Micropor. Mesopor. Mater. 22 (1998) 1.
[40] Y. Kuwahara, T. Kamegawa, K. Mori, H. Yamashita, Chem. Commun. (2008) 4783.
[41] Y. Kuwahara, K. Maki, Y. Matsumura, T. Kamegawa, K. Mori, H. Yamashita, J. Phys. Chem. C 113 (2009) 1552.
[42] T. Kawai, K. Tsutsumi, Colloid Polym. Sci. 276 (1998) 992.
[43] J. Pérez-Pariente, J. Sanz, V. Fornés, A. Corma, J. Catal. 124 (1990) 217.
[44] T. Kawai, K. Tsutsumi, J. Colloid Interface Sci. 212 (1999) 310.
[45] W.M.H. Sachtler, Z. Zhang, Adv. Catal. 39 (1993) 129.
[46] D. Brühwiler, G. Calzaferri, Micropor. Mesopor. Mater. 72 (2004) 1.
[47] A. Corma, G. Hermenegildo, Chem. Commun. (2004) 1443.
[48] Y. Xu, C.H. Langford, J. Phys. Chem. B 101 (1997) 3115.
[49] V. Durgakumari, M. Subrahmanyam, K.V. Subba Rao, A. Ratnamala, M. Noorjahan, K. Tanaka, Appl. Catal. A 234 (2002) 155.
[50] S. Anandan, M. Yoon, J. Photochem. Photobiol. C 4 (2003) 5.
[51] Y. Xu, C.H. Langford, J. Phys. Chem. 99 (1995) 11501.